Heliyon 10 (2024) e38787

Contents lists available at ScienceDirect

Heliyon

journal homepage: www.cell.com/heliyon

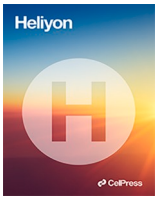

Research article

Predicting land use dynamics, surface temperature and urban thermal field variance index in mild cold climate urban area of Pakistan

Mudassir Khan [a], Muhammad Qasim [b], Adnan Ahmad [a,d], Adnan Ahmad Tahir [c,*], Abida Farooqi [a,**]

[a] Department of Environmental Sciences, Quaid-i-Azam University, Islamabad, Pakistan
[b] Department of Environmental and Conservation Sciences, University of Swat, Pakistan
[c] Department of Environmental Sciences, COMSATS University Islamabad (CUI), Abbottabad Campus, Abbottabad, 22060, Pakistan
[d] Department of Forestry, Shaheed Benazir Bhutto University, Sheringal Dir Upper, 18000, Pakistan

ARTICLE INFO

Keywords:
Artificial neural network
Cellular automata
Land cover modification
Land surface temperature
Urban heat island
Urban thermal field variance index

ABSTRACT

Rapid urbanization attributed to population growth is affecting the built environment's thermal and landscape dynamics. Using Landsat satellite datasets, this study investigated the complex interplay between urban Land Cover (LC) modification, fluctuation in Land Surface Temperature (LST) and severity of Urban Heat Island (UHI) from 1990 to 2020 in Peshawar City, Pakistan. Thermal bands were used to calculate LST and severity of UHI using the Urban Thermal Field Variance Index (UTFVI). Furthermore, through Cellular Automata (CA), Logistic Regression (LR), and Artificial Neural Network (ANN), future predictions on thermal characteristics associated with land use changes were made. The results showed that the urban areas expanded by ~25 % from 1990 to 2020, while a ~10 % decrease occurred in urban vegetation. The city is projected to expand by ~45 % and ~56 % in 2035 and 2050, respectively. Notably, the results also demonstrated that urban hotspots were found the warmest with the strongest UHI severity (~34 °C), followed by the barren land (~32 °C), and vegetation. The results further predicted an increase of LST (~55 % and ~82 %) and UTFVI (~62 % and ~83 %) in 2035 and 2050, respectively. These findings provide useful insights for policymakers and city planners to mitigate heat stress and create a sustainable urban environment through the development of effective urban land use policies and urban greening.

1. Introduction

The climate is the most significant environmental variable that is shaping the earth's biosphere and living conditions [1]. Urbanization and climate change are among the two major threats to humanity [2]. Land use land cover (LULC) changes attributed to urbanization are expanding the impervious land surface throughout the world and are causing various ecological and climatic problems. In the next three decades, it is expected that metropolitan regions of the world will consist of 70 % of the global population.

* Corresponding author.
** Corresponding author.
E-mail addresses: mudassirkhan@bs.qau.edu.pk (M. Khan), drqasim@uswat.edu.pk (M. Qasim), adnanfr@sbbu.edu.pk (A. Ahmad), Adnantahir@cuiatd.edu.pk (A.A. Tahir), abida.farrukh@gmail.com (A. Farooqi).

https://doi.org/10.1016/j.heliyon.2024.e38787
Received 21 May 2024; Received in revised form 30 August 2024; Accepted 30 September 2024
Available online 1 October 2024

Though cities cover about 2 % of the global land surface but absorb 75 % of energy. The extensive establishment activities in these urban hotspots are creating massive LULC changes, degrading the urban environment and also acting as a major source of global warming and climate change. These trends in urbanization also have the potential to impose considerable effects on the ecology, hydrology, temperature, microclimate, biodiversity, farm, and green lands of the urban landscapes.

Vegetation in urban areas is vital for the ecological health of the urban environment [3]. Vegetation maintains water and soil quality, helps in atmospheric circulation, stocks and sequesters atmospheric carbon and maintains the balance of different ecosystem services [4]. Urbanization, followed by the conversion of green surfaces into impervious surfaces, releases an enormous amount of heat [5] and causes the LST to rise [6,7]. The metropolitan areas, therefore, have higher surface temperatures compared to the surrounding rural areas [8]. This phenomenon is called the Urban Heat Island (UHI) effect [9]. The UHI attributed to the conversion of vegetated surfaces into roads, residential and commercial infrastructures coupled with the heat produced by heavy traffic, factories, aerosols, fuel stations and air conditioning systems [10] is the direct indicator of ecological, socioeconomic and human health deterioration. The increased energy consumption for air conditioning and their associated greenhouse emissions are their additional repercussion [11, 12].

Urban Thermal Field Variance Index (UTFVI) is an indicator that is used by many scientists to describe the effect and severity of UHI in thermal conditions of urban environments [13–15]. The composition, distribution, and configuration of LULC types can influence the magnitude and severity of LST [16]. In particular, the arrangement of landscape elements such as shape, structure, and spatial layout of the buildings cause variation in LST [16,17]. The towering and congested buildings, small roadways and minimum green area reduce wind speed and longwave radiation, increase reflection, shortwave radiation and evapotranspiration, followed by urban landscape warming [18]. High UTFVI deteriorates the quality of urban ecology, environment, and well-being of the residents by changing the local winds and humidity pattern, changes in air quality and pattern of rainfall, etc. [19–21]. Numerous studies analyzed the effect of LULC and urbanization on LST and UTFVI using remote sensing data. Rapid urbanization-based LULC change has led to significant changes in the urban thermal environment by replacing vegetative cover with impervious surfaces. A study [8] indicated the impact of urbanization on temperature variation using MODIS datasets and neural networks. The study showed a 5 % increase in urbanization which increased LST and UTFVI in Northern Iran. A study [22] using Landsat datasets and a linear regression model showed an increase of 7.9 °C LST due to urbanization, a decline in vegetation and about 45.8 % of the area was found worst with the strongest UTFVI. Another study [23] in the Dhaka metropolitan area showed that the strongest UTFVI would cover ~72 % of the area which was 58 % in 2020. A study conducted in Lahore, Pakistan using simple linear regression showed the intensification of UHI and increase in mean surface temperature by 4.5 °C in 2000 and by 5.9 °C in 2020 [24].

UHI associated with LULC, and their related consequences have greater importance among the global scientific community. The results of the studies across the globe concluded that LULC has significant adverse effects on the LST and causes environmental, ecological and health-related problems in the urban regions of developing and developed countries [16,25–28]. However, global studies lack the gradient direction analysis (GDA) and this gap is addressed in this study by incorporating GDA to assess both the distance and direction from center of the city where urbanization is increasing and analyze the associated variations in LST. GDA provides detailed understanding of the existing pattern of urbanization and their related thermal effect. Additionally, this study analyzes the influence of induced urbanization due to war and conflicts which consequently affects the thermal conditions of a region by changing the LULC.

Since the last four decades, urbanization has drastically increased and this rate is found to be much faster in developing countries like Pakistan than the developed countries [29]. The major cities in Pakistan such as Islamabad, Karachi, Lahore, and Peshawar are facing rapid urbanization. In Pakistan, green areas are decreasing at the rate of 0.75 % and the increase in urbanization rate is about 3

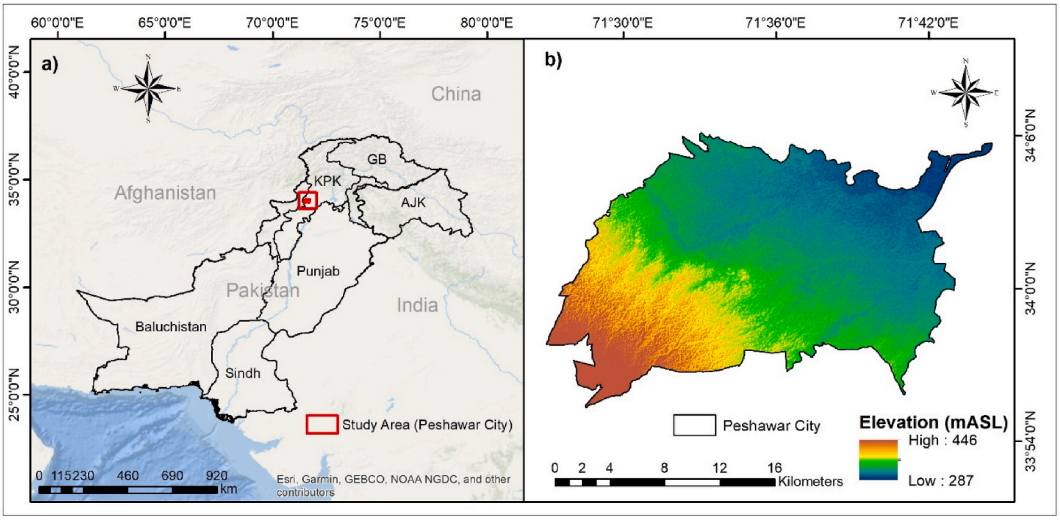

Fig. 1. Location (a) and elevation (b) of the study area (Peshawar City).

% [30]. The vegetation type within the city, surrounding urban areas and mountains provides biodiversity hotspots, stores, and sinks huge amounts of carbon and plays a vital role in the hydrological and ecological balance. Peshawar City bears tropical thorns, and deciduous types of vegetation and the surrounding hills of Khyber Mountains bear sub-tropical vegetation. The city faced a huge influx of Afghan refugees and internally displaced people during the Russian invasion in the 1980s, post 9/11 war and Pakistan's war on terror which induced massive LULC change. The LULC-induced LST and its related UHI not only affects the socio-economic situation, ecology, hydrology, health and biodiversity of the urban environment, but it also poses potential threats to the surrounding rural regions. The UHI associated with increased LST in the city also affects the ecosystem services of the natural landscape. Therefore, it is required to track and predict how LULC will affect the LST, UHI, and UTFVI concerning the above-mentioned gaps. This study will be helpful in the development of the city's land management plan and policies to restrict unplanned urbanization and promote urban greening to mitigate UHI consequences.

2. Materials and methods

2.1. Study area

Peshawar is the largest city of Khyber Pakhtunkhwa (KP) province of Pakistan and serves as the provincial capital. It lies between 33°55′ and 34°60′ North Latitude and 71°22′ and 71°43′ East Longitude (Fig. 1). Peshawar city is situated in the mild cold climatic zone of Pakistan [31]. In summer, the mean maximum temperature exceeds 40 °C and the mean minimum temperature is close to 25 °C. The month of March marks the beginning of spring when the weather is pleasant. Precipitation occurs in both winter and summer. In winter, the western disturbance causes severe rainfall from February to April. The highest average precipitation in winter occurs in March while the highest average summer precipitation due to monsoon intrusion is recorded in August. Precipitation is higher in winter as compared to summer.

Peshawar city is situated in proximity to the Hindukush Mountain ranges of Pakistan. The city shares a border with the war-affected Afghanistan from the West and the internally war-effected region of Waziristan from the South-West. The city has been facing rapid urbanization associated with population growth, migration of rural communities, a huge flow of internally displaced people, and a massive flow of Afghan refugees. The city has been ranked one of the most unplanned cities, lacking an ordered and well-planned land use management and infrastructures.

2.2. Data Acquisition and pre-treatment

Three different satellite sensors were selected to acquire Landsat satellite data (i.e., Landsat 5-TM, 7-ETM+ and 8-OLI), from the Earth Explorer Data Portal of United States Geological Survey (USGS) for the summer season (June–August) of years 1990, 2005 and 2020 to assess the past fluctuation in LULC, LST, and UHI. Cloud cover in the selection criteria was set at <10 % before downloading the selected satellite imageries to minimize the classification uncertainties and maximize the accuracy (Table 1).

Standard procedures of data treatment were applied in QGIS software before land use classification and LST derivation. The treatment procedures include atmospheric correction, gap-filling (specifically related to Landsat 7-ETM+) and radiometric calibration. LULC, LST and UTFVI change analysis was carried out using ArcGIS, QGIS and ENVI software after the data pre-treatment process.

2.3. Classification of LULC change for the period 1990 to 2020 and its accuracy assessment

All the satellite imageries were classified into five classes (built-up, bare soil, vegetation, agriculture, and water bodies). LULC classification methods are divided into three major types i.e., supervised, unsupervised and object-based classification. Supervised classification was used to classify satellite imagery in this study. The Artificial Neutral Network (ANN) algorithm was used for the classification process utilizing ENVI software. Theoretically, ANN is a sophisticated and more robust classification method. ANN gives higher accuracy even with fewer training samples [32]. The capability of ANN to handle complex, non-linear relationships in different LULC classes makes it more effective to identify complex patterns in remote sensing data [33]. ANN showed higher classification accuracy compared to classical algorithms i.e., Maximum Likelihood or Decision Tree etc. [33,34]. A total of 35–40 samples were selected for each LULC class for training and testing purposes. Accuracy assessment was done after the classification of all the imageries. Confusion matrix and kappa index were used to measure the accuracy using equations (1)–(4) [23] because these are considered the best methods.

Table 1
Details of the downloaded Landsat images.

Year	Platform	Sensor	Resolution	Path/Row	Cloud Cover
1990	Landsat-5	TM	30 m	151/36	<10 %
2005	Landsat-7	ETM+	30 m	151/36	<10 %
2020	Landsat-8	OLI	30 m	151/36	<10 %

(Source: US Geological Survey).

$$\text{User's accuracy, U.A (\%)} = \left(\frac{y_{mm}}{y+m}\right) \times 100 \tag{1}$$

$$\text{Producer's accuracy, P.A (\%)} = \left(\frac{y_{mm}}{y_{m+}}\right) \times 100 \tag{2}$$

$$\text{Overall accuracy, O.A} = \frac{1}{N}\sum_{m=1}^{j} n_i \tag{3}$$

$$\text{Kappa coefficient (K)} = \frac{N\sum_{m=1}^{j} y_{mm} - \sum_{m=1}^{j} (y_{m+1} \cdot y_{+m})}{N^2 - \sum_{m=1}^{j} (y_{m+1} y_{+m})} \tag{4}$$

2.4. Estimation of LST for the years 1990, 2005 and 2020

LST was estimated using the information stored in thermal bands of the selected satellite images for the years 1990, 2005 and 2020, respectively. Band 6 and 10 were used for Landsat 5, 7, and 8, respectively. Landsat Satellite acquired thermal data which is stored in Digital Numbers (DNs) format. LST is calculated from these DNs by using the following set of equations (5)–(8) [35] in this study.

2.4.1. Conversion of digital numbers (DNs) into radiance

Radiance was calculated from digital numbers using Equation (5).

$$L\lambda = \frac{(\text{LMIN} + (\text{LMAX} - \text{LMIN})\text{x DN})}{255} \tag{5}$$

Where "Lλ" is the Spectral Radiance; "LMIN = 1.238" & "LMAX = 15.30" for Landsat 5; "LMIN = 1.238" & "LMAX = 15.600" for Landsat 7; and "LMIN = 0.10033" & "LMAX = 22.00180" for Landsat 8.

2.4.2. Calculation of brightness temperature (TB) from radiance

Brightness temperature (*TB*) was calculated from radiance using Equation (6).

$$TB = \frac{K2}{In\left((K1/L\lambda) + 1\right)} \tag{6}$$

Where;

"TB" = Brightness temperature (in Kelvin) at sensor; K1 & K2 = Calibration Constants, which have the given specific values for the given Landsat sensors; *"K1 = 607.76" & "K2 = 1260.56"* for Landsat 5; *"K1 = 666.09" & "K2 = 1282.71"* for Landsat 7; *"K1 = 774.89" & "K2 = 1321.08"* or band 10 of Landsat 8; *"K1 = 480.88" & "K2 = 1201.14"* for band 11 of Landsat 8.

2.4.3. Conversion of TB (in Kelvin) into Celsius (^oC)

The calculated brightness temperature (in Kelvin) was transformed into a Degree-Celsius scale (^oC) using Equation (7).

$$TB\ (^\circ C) = TB\ (in\ Kelvin) - 273.15\ (K) \tag{7}$$

2.4.4. Calculation of Land Surface Temperature (LST) from TB (^oC)

LST was finally calculated from brightness temperature using Equation (8).

$$LST = \frac{\text{TB}}{([1 + (\lambda * \text{TB}/\rho) * \ln(\varepsilon)])} \tag{8}$$

Where.

λ = emitted radiation.
ρ = H*C/S
H = 6. 626 * 10^{-34}J/s (Planck's constant)
S = 1.38*10^{-23}J/K (Boltzmann constant)
C = 2.998*10^{8} m/s (Speed of Light)
ε = Surface emissivity

Surface emissivity is required to calculate the final LST. The proportion of vegetation (PV) was used to estimate surface emissivity. The PV is calculated using the vegetation index for the years 1990, 2005 and 2020, respectively. Equation (9) [36] was used to calculate PV.

$$PV = [(NDVI - NDVI_{min})/ (NDVI_{max} - NDVI_{min})]^2 \tag{9}$$

Surface emissivity was estimated using Equation (10) [36].

$$Surface\ emissivity\ (\varepsilon) = 0.004^{*}\ PV + 0.986 \tag{10}$$

2.4.5. LST Standardization

Standardization is required to overcome the effect of topographical, seasonal, and climatic variations which cause biases. Therefore, it is not appropriate to compare directly the variation in LST for several years. The calculated LST was therefore standardized for the years 1990, 2005 and 2020 by using Equation (11) [37].

$$LST_{\beta} = \left(\frac{LST_{\rho} - \overline{LST_{\alpha}}}{LST_{\delta m}}\right) LST_{\pounds i} + \overline{LST_{z}} \tag{11}$$

Where.

LST_{β} = pixel specific normalized LST for the year y (=1990 or 2020).
LST_{ρ} = pixel specific LST before normalization.
$\overline{LST_{\alpha}}$ = image specific mean LST either for the year 1990 or 2020.
$LST_{\delta m}$ = image specific SD (standard deviation) of LST either for the years 1990 or 2020.
$LST_{\pounds i}$ = image specific SD of LST of reference year i (=2005).
$\overline{LST_{z}}$ = image specific mean LST for the year 2005.

2.4.6. LST zonal classification

The standardized LST was divided into six different classes i.e., "<25 °C", "25–28 °C", "28–30 °C", "30–33 °C" and ">33 °C". This categorization was done to assess the areal distribution, trend, and spatial variation in each temperature class from 1990 to 2020 in Peshawar City.

2.5. Urban thermal field variance index (UTFVI)

The urban thermal field variance index (UTFVI) is an indicator that evaluates the thermal and environmental quality of urban areas. UTFVI is a widely used index that describes the UHI effect more precisely. This index shows the spatial variability of LST and UHI in urban areas where the temperature is higher as compared to the surrounding rural areas. This index is calculated using the LST values of the respective years as given in Equation (12) [22]. This index is divided into six different classes (None, Weak, Medium, Strong, Stronger, Strongest) based on the presence of urban heat intensity and its effects on the urban thermal environment and human well-being.

$$UTFVI = \frac{T_s - T_m}{T_s} \tag{12}$$

Where; T_s = pixel-specific LST, and T_m is the LST mean for the study area.

2.6. Gradient-direction (GD) estimation

GD analysis is a procedure used to summarize the spatio-temporal pattern of LULC and LST at the microscale. This process is called upscaling microscale [38]. Firstly, concentric rings were created from the center of the city at constant intervals. The outermost concentric ring should cover the whole study area to incorporate all the LULC (specifically urban area) and LST classes. Secondly, the 16 possible directions were drawn from the city center. All the directions were divided by concentric zones in a series of gradients. Finally, urbanization and LST were represented by all the possible gradient segments to estimate the variations in LULC and LST at several directions and distances.

2.7. Prediction of the future LULC, LST and UTFVI changes for years 2035 and 2050

Several models are used for the future prediction/simulation of LULC and LST changes. The selection of a suitable simulation model depends on the individual's context or objectives of the study e.g., the procedure of land modification, the availability of datasets, the direction of research, and the validity of the prediction process [39,40]. In this research, CA-LR and ANN models were used for the future prediction/simulation of changes in LULC, LST and UTFVI for the years 2035 and 2050. These models' algorithms detect the hidden pattern within the past data and predict the future variables accordingly. Therefore, the interval between the past (1990, 2005, and 2020) and future (2035 and 2050) years were kept same i.e. 15 years.

The input parameters of the models consist of dependent variables (LULC change map and LST distribution map) and independent variables, i.e., distance from roads, residential, commercial, and educational places, elevation and slope (for LULC simulation), Normalized Difference Vegetation Index (NDVI), Normalized Difference Built-up Index (NDBI) and Normalized Difference Water Index (NDWI) (for LST simulation), changes in LULC and changes in LST (for UTFVI simulation).

The variation in LULC and LST was calculated between two time periods to create transition matrices. The module was first trained

using LR and ANN algorithms and then CA was used to predict the future LULC, LST and UTFVI for the years 2035 and 2050. MOLUSCE plugin tool available in the QGIS software was used to predict the LULC and LST changes (through ANN and CA) for this study. This tool is considered to be among the best prediction models. ANN uses equation (13) to predict LST [13] as given below:

$$LSTy = K_2\left(\sum_{j=1}^{l} \omega_j^{(2)} \cdot K_1\left(\sum_{i=1}^{n} \omega_i^{(1)} \cdot x_i + \varphi_j^{(1)}\right) + \varphi^{(2)}\right) \quad (13)$$

Where.

$LSTy$ = predicted LST for a future year based on the past pattern
K_1 and K_2 = activation functions for hidden and output layers.
$\omega_i^{(1)}$ and $\omega_j^{(2)}$ = weights of input to hidden and hidden to output layers.
$\varphi_j^{(1)}$ and $\varphi^{(2)}$ = bias terms for hidden and output layers.

During the accuracy validation process, different kappa statistics were generated (such as percent of correctness, standard kappa, etc.). All explanatory variables were placed in a common group, which can model all transitions effectively. This was done because the driving forces for all the transitions were the same [39]. The estimated changes in land cover (such as the transitions from other LULC types to built-up areas) were used as the dependent variables in the first step; whereas in the second step, other spatial variables like distance to roads, water body, vegetation, bare soil, slope, and elevation were considered as independent variables.

The models were first trained on a known dataset for a specific period i.e. model trained for LULC, LST and UTFVI datasets over the year 2020. CA model was validated by comparing the actual and predicted LULC for the year 2020 with an overall kappa value (K) of 0.84. The accuracy of ANN was assessed by comparing the observed and simulated LST and UTFVI for the year 2020. The model was used for future prediction once a high correlation coefficient (R) value of 0.89 and Root Mean Square Error (RMSE) value of 0.32 were achieved.

3. Results

3.1. Land use Land cover change and Land Surface Temperature dynamics

The accuracy of classified images using the Kappa coefficient (for the years 1990, 2005 and 2020) and the accuracy of LULC classes using the confusion matrix are shown in Tables 2 and 3, respectively. All the available images were accurately classified with a Kappa coefficient value of ≥0.90 and an overall accuracy of ≥92 % for all data years (Table 2).

The accuracy of the classified LULC was assessed by using a confusion matrix. The matrix shows a user accuracy (UA) of ≥0.92 and a producer accuracy (PA) of ≥0.92 (Table 3). It shows that the LULC classes are assessed accurately using ANN in ENVI software.

Areal changes in LULC and LST are presented in Table 4 and Fig. 2. Over the different periods, major shifts in the LULC are clear. Most importantly, a drastic increasing trend in the built land and reduction in vegetation and bare soil was found (Table 4). A net reduction in the agricultural land and water bodies was also found. The LST pattern during the respective periods also shows an incredible shift (Fig. 2).

The transition matrix showed 45.20 km^2 area was converted from bare soil to a built-up area (Table 5). The second highest conversion to built-up area was noted from agriculture to built-up which is 24.28 km^2 during the study duration. Vegetation and agriculture to bare soil showed 20.39 km^2 and 27.88 km^2, respectively, in the study area. These are the green spaces in the proximity of the city center which were converted to bare soil. A total of 11.37 km^2 baren areas were converted to vegetation in the study area.

The area associated with high temperature (i.e., above 33 °C) was 9.10 % in 1990, which was increased to 38.90 % in 2020. Similarly, over the period, the area concerned with a temperature range between 30 and 33 °C increased from 31.01 % to 46.82 %, while the area having a temperature range from 25 to 28 °C dropped from 32.70 %) to 0.87 % [Fig. 3(G)]. Among the different land use classes, urbanized areas have the highest mean surface temperature, followed by bare soil, agriculture, and vegetation [Fig. 3(I)].

The results in Fig. 3(I), further showed a continuous increase in LST among all classes. The spatial behavior of LST showed temperature variation when moved in different directions while crossing the city center. The analysis showed [Fig. 3(H)] the highest temperature in the city center as compared to the adjacent areas. The area highlighted in the blue rectangle [Fig. 3(H)] is the city center when moved from different directions. Taken together, between 1990 and 2020, a significant expansion occurred in the built environment (25 %), while vegetation surface and bare soil decreased drastically (9 and 10 %, respectively). Similarly, high and moderate-temperature areas expanded by 30 and 15 %, respectively, while a 30 % decrease occurred in the low-temperature zone.

Table 2
Accuracy assessment of the classified images for the years 1990, 2005 and 2020.

Year	User Accuracy (U.A) (%)	Producer Accuracy (P.A) (%)	Overall Accuracy (%)	Kappa coefficient
1990	93.35	92.56	92.95	0.90
2005	94.13	93.85	93.99	0.91
2020	94.58	93.82	94.20	0.91

Table 3
Confusion matrix to estimate the accuracy of LULC classification.

Referenced LULC classes							
LULC Class	Built-up	Bare soil	Vegetation	Agriculture	Water	Total	UA (%)
Built-up	29	1	0	1	0	31	94
Bare soil	1	37	1	0	1	40	92
Vegetation	0	0	34	1	1	36	94
Agriculture	0	1	1	33	0	35	94
Water	1	0	0	1	30	32	93
Total	31	39	36	36	32	174	
P.A (%)	94	94	94	92	93		93

Table 4
Land use land cover (LULC) change for the years 1990, 2005 and 2020.

Class name	1990 (km^2)	2005 (km^2)	2020 (km^2)	Change (%)		
				(1990–2005)	(2005–2020)	(1990–2020)
Built-up	20.95	54.90	99.67	+10.85	+14.31	+25.16
Bare soil	113.99	133.90	86.55	+6.36	−15.13	−8.77
Vegetation	79.47	31.92	47.45	−15.20	+4.96	−10.24
Agriculture	95.37	90.10	78.03	−1.69	−3.86	−5.54
Water bodies	2.93	2.08	1.02	−0.27	−0.34	−0.61

3.2. Analysis of gradient-direction of urban sprawl, green spaces and UHI

Gradient-direction analysis showed that the city is expanding between "W" and "S" gradients from 1990 to 2020. The "SW" gradient showed a 12 km expansion in urban areas from the city center (Fig. 4).

The analysis further showed a decreasing trend in urban green spaces from 1990 to 2020. A 15 % decline was shown from 1990 to 2005 in urban green spaces. A slight increase in urban green spaces was found from 2005 to 2020. This increase may be due to the initiation of the Billion Tree Tsunami Afforestation Project (BTTAP) by the KP government. Overall, a 10 % decline in urban green spaces was analyzed from 1990 to 2020. Maximum decline in green spaces was shown between "S" and "W" gradients. The results in Fig. 4 further provide evidence that urbanization in Peshawar City was maximum in the first concentric zone, expanding 2 km from the city center. In 1990, a slight increase in urbanization in the "SW" gradient was found and the highest LST (>33 °C) was recorded in all gradient-directions from the city center up to 2 km (Fig. 5). The analysis in Fig. 5 showed that the city is expanding in "SW" and "WSW" alternatively raising in temperature within 6–12 km.

The analysis in Fig. 5 showed an increasing trend in urbanization in "SW" and "WSW" gradients from the city center, which caused the increase in LST in the same direction gradients (Fig. 5). Notably, a prominent increase was found between "S" and "W" gradients in 2005–2020 (Fig. 5). The highest LST was also recorded in the same direction gradient due to the expansion of the city and reduction in urban green spaces.

3.3. Variation in urban thermal field variance index (UTFVI)

The urban thermal field variance index (UTFVI) shows the intensity or severity of urban heat in the study area. The results showed an increasing trend in urban heat intensity throughout the study duration (Table 6 and Fig. 6). According to the results, a decreasing trend is apparent in the "None" UTFVI region, while a significant upward trend in the strong, stronger, and strongest effect was recorded. Overall, from 1990 to 2020, the area of no effect decreases from 253 km^2 to 156 km^2, while the area of strongest effect increases from 57 km^2 to 125 km^2.

The results revealed that the intensity of urban heat is maximum at the city level but there was no severe effect found in the surrounding non-urban areas attributed to more green spaces (Fig. 6). According to the results, a +21.73 % increase occurred in the highest UTFVI class where the lowest class showed a significant decrease.

3.4. Projected future LULC, LST and UTFVI dynamics

According to the simulation, approximately 10.22 % and 12.32 % of the area will be transformed into an urban or built-up environment [Table 7, Fig. 7(I)] by 2035 and 2050, respectively. In a similar fashion to LULC, the LST also changed (Fig. 2) during the study period (1990–2020). Therefore, the LST for the future period (2035 and 2050) was also simulated, as shown in Fig. 7. The ANN model was used to predict future LST trends in Peshawar City using past data. Due to the strong correlation of LULC with LST, the map shows an increasing trend that will affect the temperature. The simulation shows that about 68 % and 88 % of the study area will experience high temperatures (>28 °C) by 2035 and 2050, respectively (Table 7), compared to 48.47 % in 2020.

Future prediction on UTFVI for the years 2035 and 2050 is shown in Fig. 8 and Table 8, showing an alarming scenario. The results

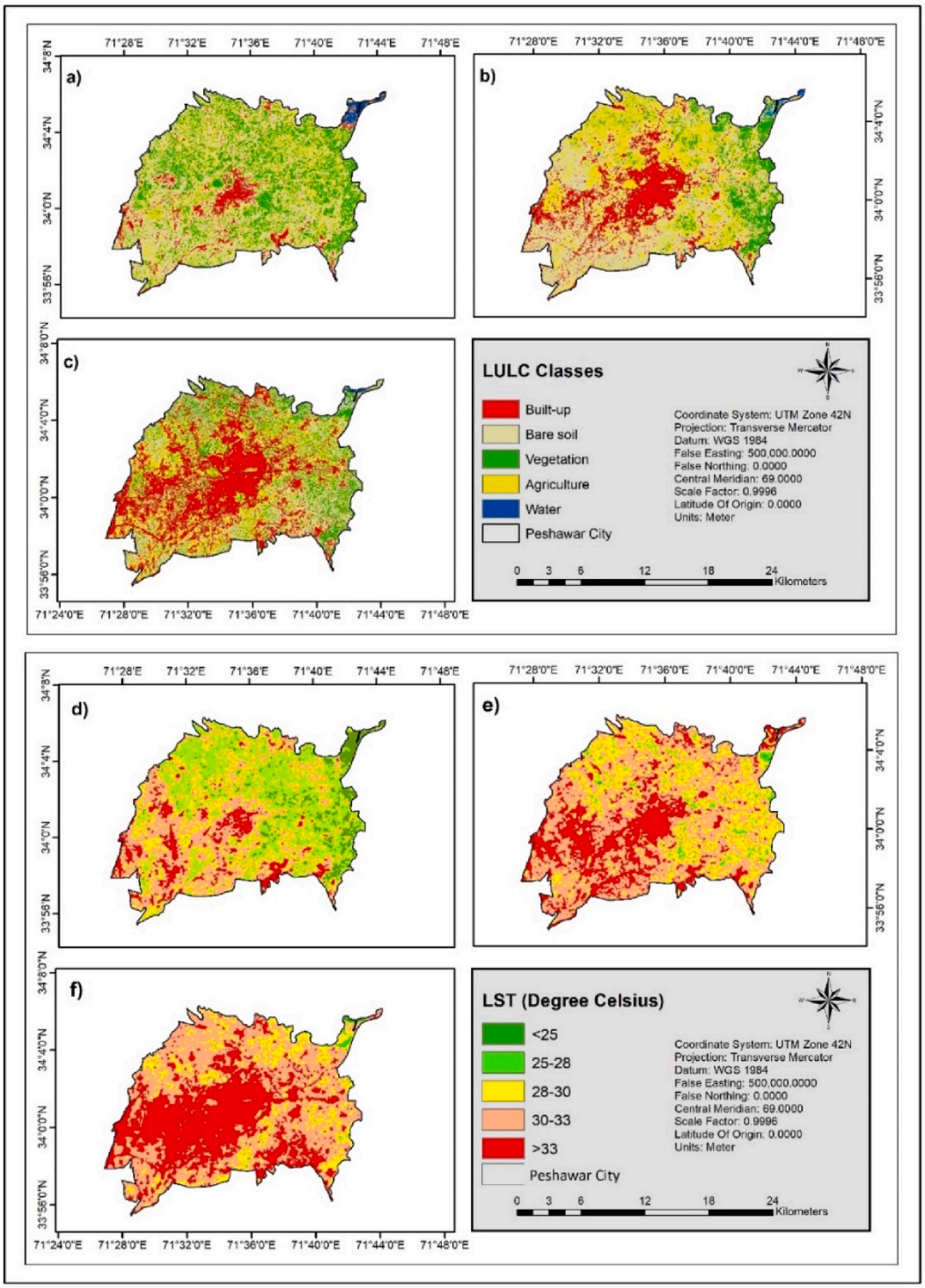

Fig. 2. LULC (a–c) and LST (d–f) changes for years 1990, 2005 and 2020 in the study area.

show a decreasing trend in low UTFVI and an increasing trend in high UTFVI. None and weak UTFVI class will reduce by 6 % and 2.56 %, respectively, while the highest UTFVI class will be 61.66 % and 83.07 % in 2035 and 2050, respectively. These assessments concluded that LULC and related LST increases will occur in the future, which will induce UHI and will have severe effects on the urban environment.

Table 5
Transition matrix of different LULC classes (km^2) from 1990 to 2020.

LULC class	Built-up	Bare soil	Vegetation	Agriculture	Water
Built-up	14.29	3.61	0.04	0.89	0.01
Bare soil	45.20	33.28	11.37	3.95	0.01
Vegetation	15.80	20.39	17.56	5.64	0.00
Agriculture	24.28	27.88	16.67	26.42	0.01
Water	0.04	1.10	0.11	0.07	0.54

4. Discussion

4.1. LULC change dynamics

This study tracts and predicts the LULC, LST, UHI and UTFVI pattern using GIS and remote sensing, in Peshawar, the capital city of KP. The accuracy of the past LULC maps was evaluated through kappa statistics i.e. user, producer, and overall accuracy for the years 1990, 2005 and 2020. The overall classification accuracy was recorded at 94 %, 93.4 % and 93.7 %, respectively (Tables 2 and 3), highlighting strong accuracy agreement as also given in several other studies [30,45].

The LULC dynamics (Table 4, Fig. 2) showed major shifts and significant expansion in the built area at the cost of vegetation, barren land, agricultural land and water bodies. The most pronounced increase in the built-up area occurred during 2005 and 2020 (14.3 %). Similarly, a major decrease in barren land (15.3 %) was recorded between 2005 and 2020, while it was 15 % for vegetation during 1990 and 2005. However, vegetation cover expanded by 4.96 % during 2005 and 2020 which is attributed to the plantation drive under the Billion Tree Tsunami Afforestation Project (BTTAP) launched in 2013 as also indicated by Ref. [46].

Major factors that cause changes in land use are urbanization due to population growth, economic and technological development, and other environmental changes [41–44]. Urban heat island (UHI) associated with rapid urbanization is one of the major climate problems across the globe. Various major drivers are responsible for this shift in LULC in the study area (Peshawar). The area is the province's most diverse metropolis, industrialized, financial and commercial hub [40]. It also hosts the largest number of expatriates and receives the largest number of migrants from rural areas [47]. The city is also a first choice for the internally displaced people from neighboring war-on-terror-affected districts such as Waziristan, Swat, Bajaur and Dir. Furthermore, the city is sharing a border with Afghanistan (a war-affected country since the 1980s) at Torkham (66 km away from Peshawar). The city hosted a huge flow of Afghan refugees, since 1990 during different wars. Being a central hub for economic and cultural growth and a huge influx of Afghan refugees and IDPs during war periods, the city has expanded drastically and engulfed a huge amount of barren land, vegetation surface, agricultural land and water bodies.

4.2. Variation in Land Surface Temperature (LST) and urban thermal field variance index (UTFVI)

With the major shifts in the LULC, changes in LST are apparent (Table 5, Fig. 2). The increase in high and moderate temperature zones and reduction in low-temperature regions clearly explain LST variation. From all directions towards the city center, temperature is increasing [(Fig. 3(H)]. The emission characteristics of different land surfaces and building materials are different. These building materials in the built environment trap and slowly release solar energy, resulting in an increase in LST [27,48,49] and creating UHI. The gradient analysis in Fig. 5 shows an increasing LST change in SW direction, which is attributed to the rapid urbanization in the same direction as highlighted in Figs. 4 and 5. This rapid urbanization and increasing LST in SW direction is attributed to the construction of huge housing societies (like Hayatabad) educational institutions, health and industrial complexes and other buildings.

The reduction in vegetation and urban green spaces affects LST and UHI dynamics. Through shade and cooling effect, trees in urban areas create "Cold Island" [50,51]. On the other hand, a decrease in the vegetation cover can effectively increase the LST and UHI severity [2]. The analysis in Figs. 4 and 5 clearly shows that areas where green spaces are reducing bear the highest LST. However, the vegetation cover in the city showed a slight increase of 4.5 % (Table 2) since 2005, because of Billion Tree Tsunami Afforestation Project (BTTAP). Nevertheless, LST in all land uses is increasing even in green spaces. The major reasons are the drastic loss of 15 % vegetation cover (during 1990–2005) and uncontrolled urbanization. Moreover, green spaces under the BTTAP covered only selected areas, not the whole city. Furthermore, the cooling effect produced by the trees is affected by the morphological characteristics of the buildings and trees. Unplanned and poorly designed buildings, tree height, tree species, tree health, tree crown cover, stem density and the deciduous or evergreen habits of trees can affect cooling [2]. Studies showed that the greater the value of NDVI (more tree area), more will be the cooling intensity [38]. Similarly, it is reported that every 1-m increase in the tree height can reduce temperature by 0.19 °C [2]. During the BTTAP, no attention was made to the tree morphological characteristics, species selection, tree health and vigor. These morphological contracts coupled with unplanned and congested buildings in the city are preventing the trees from producing their potential cooling effect.

The rapid urbanization and their associated LULC are not only causing an increase in the LST but also resulting in the loss of various ecosystem services such as food production, native diversity, climate regulation and water supply. Regions with high LST exhibit the worst ecological status [27,52]. The conversion of forest, barren and agricultural lands will affect the ecology of these land types particularly, the conversion of forest land. The average Carbon stock by the natural vegetation type that existed in the area was estimated about 30–60 Mg C ha^{-1} [30,53]. The conversion of forest land into built-up area or other land classes can reduce the Carbon

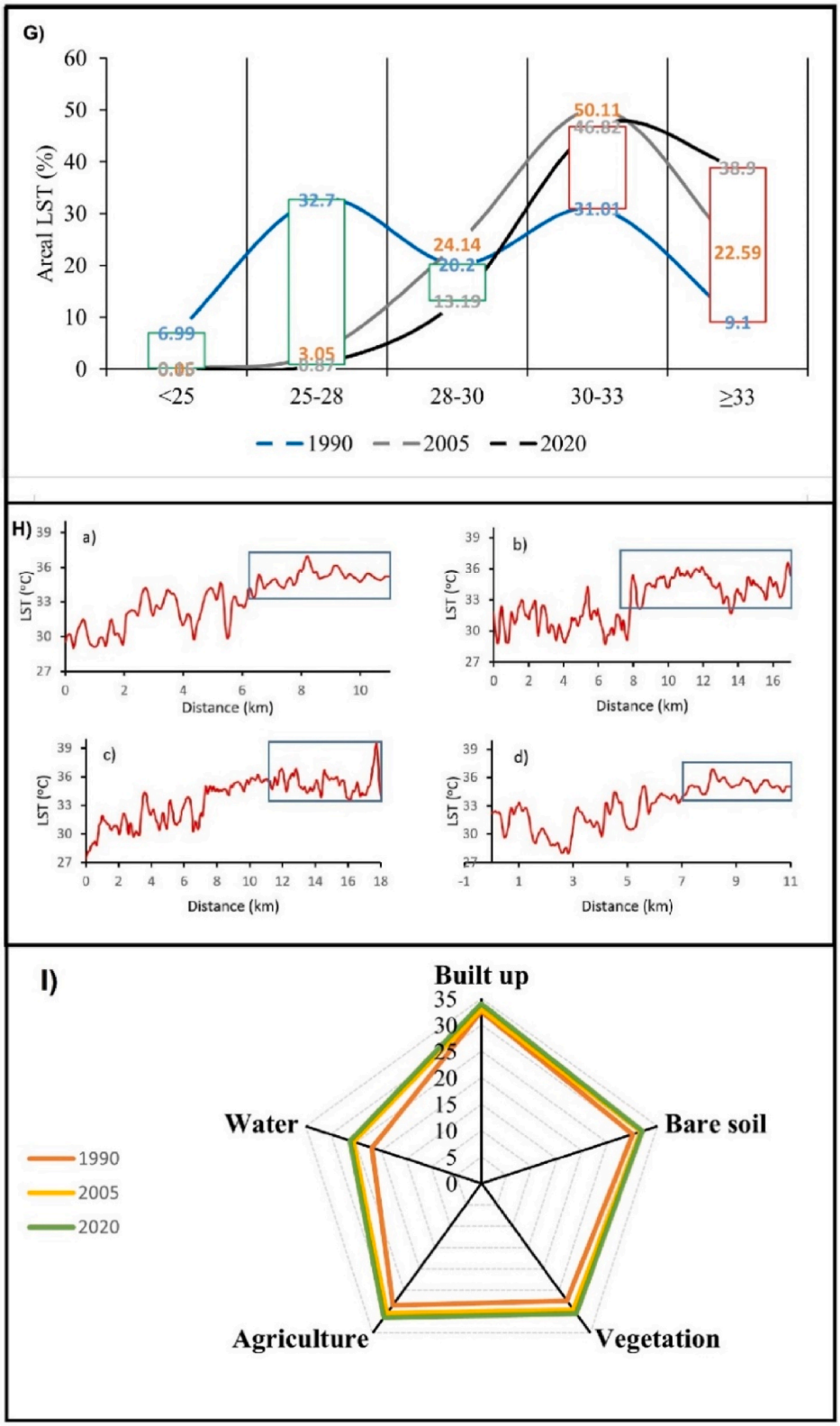

Fig. 3. [G] Area distribution trend (%) under different LST (^{o}C) classes, [H] Aspect-wise LST behavior from **a)** N to S, **b)** E to W, **c)** NE to SW and **d)** NE to SE directions, and [I] Variations in mean LST (^{o}C) over different land cover classes in the study area.

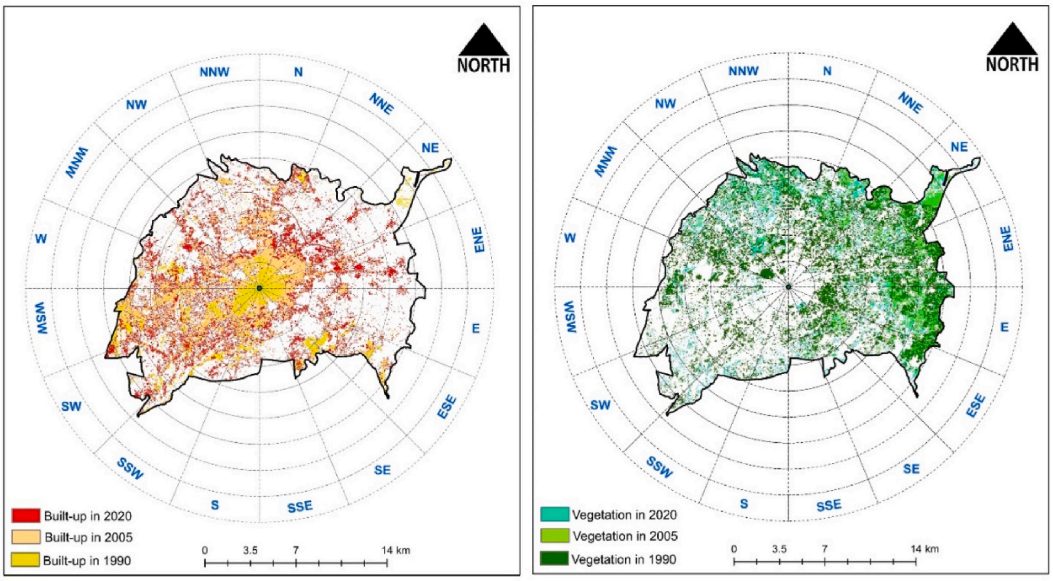

Fig. 4. Gradient-direction estimation of urban expansion (left panel) and vegetation reduction (right panel) from 1990 to 2020.

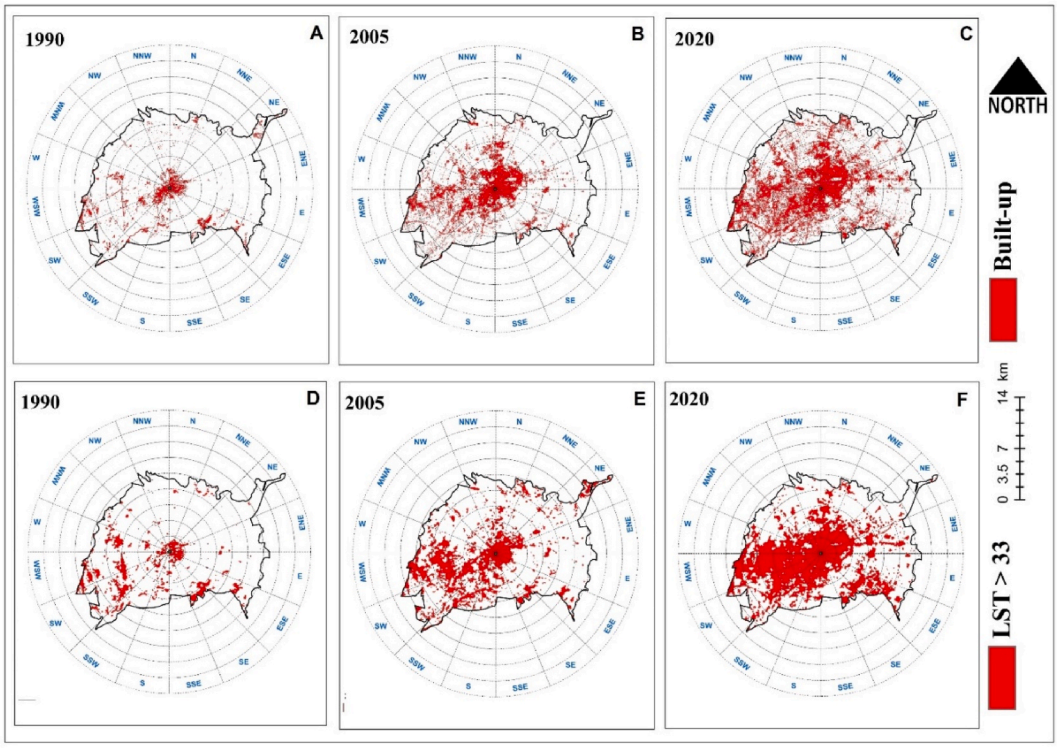

Fig. 5. Spatial distribution of urban area (A, B, C) and LST >33 °C (D, E, F) in 1990, 2005 and 2020.

stock and sequestration potential by 50–80 % [14,30,54].

4.3. Projected LULC, UHI and UTFVI

The CA model was used to predict changes in LULC for the years 2035 and 2050 [Fig. 7(I)] which predicts the scenario of each cell by using the past pattern of a cell from a neighborhood as per the standardized transition rules [55]. Thus, assuming the LULC change

Table 6
Changes in UTFVI from 1990 to 2020 in the study area.

UTFVI	Area (km^2)			Change (km^2)			Net Change (%)
	1990	2005	2020	1990–2005	2005–2020	1990–2020	1990–2020
None	243	194	156	−49	−38	−87	−27.80
Weak	0.3	14	8	+13.7	−6	+7.7	+2.46
Middle	11.7	4	8	−7.7	+4	−3.7	−1.18
Strong	0.4	14	8	+13.6	−6	+7.6	+2.43
Stronger	0.6	2	8	+1.4	+6	+7.4	+2.36
Strongest	57	85	125	+28	+40	+68	+21.73

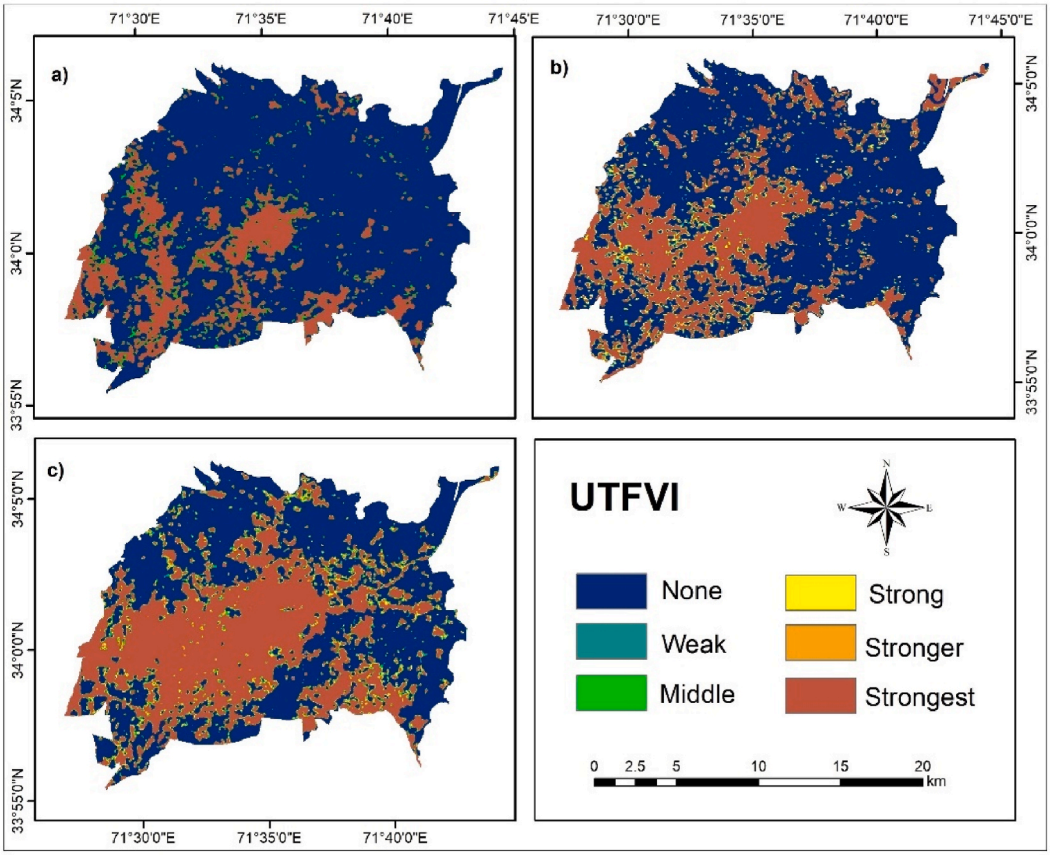

Fig. 6. UTFVI map of the study area for the years a) 1990, b) 2005 and c) 2020.

Table 7
Projected area changes in LULC and LST for the years 2035 and 2050.

LULC Class	Area (%)		LST Classes	Area (%)	
	2035	2050		2035	2050
Built up	45.00	55.55	<25 °C	0.14	0.12
Bare soil	26.43	24.08	25 °C–28 °C	0.45	0.39
Vegetation	10.42	8.79	28 °C–30 °C	2.97	2.90
Agriculture	17.82	11.36	30 °C–33 °C	41.52	14.01
Water bodies	0.26	0.15	≥33 °C	54.84	82.41

rate to be constant, the future change of LULC can be reliably predicted. The projected shifts in LULC [Table 4 and Fig. 7(I)] showed a significant increase of 22 % in the built environment and an 18 % reduction in vegetation is expected by 2050. These drastic shifts in the LULC will affect the future LST. Compared to a 38 % increase in the highest LST class between 1990 and 2020 (Fig. 3), the projected increase is estimated to be 82 % by 2050 (Table 7). Furthermore, by 2050 a drastic expansion in the stronger and strongest UTFVI is

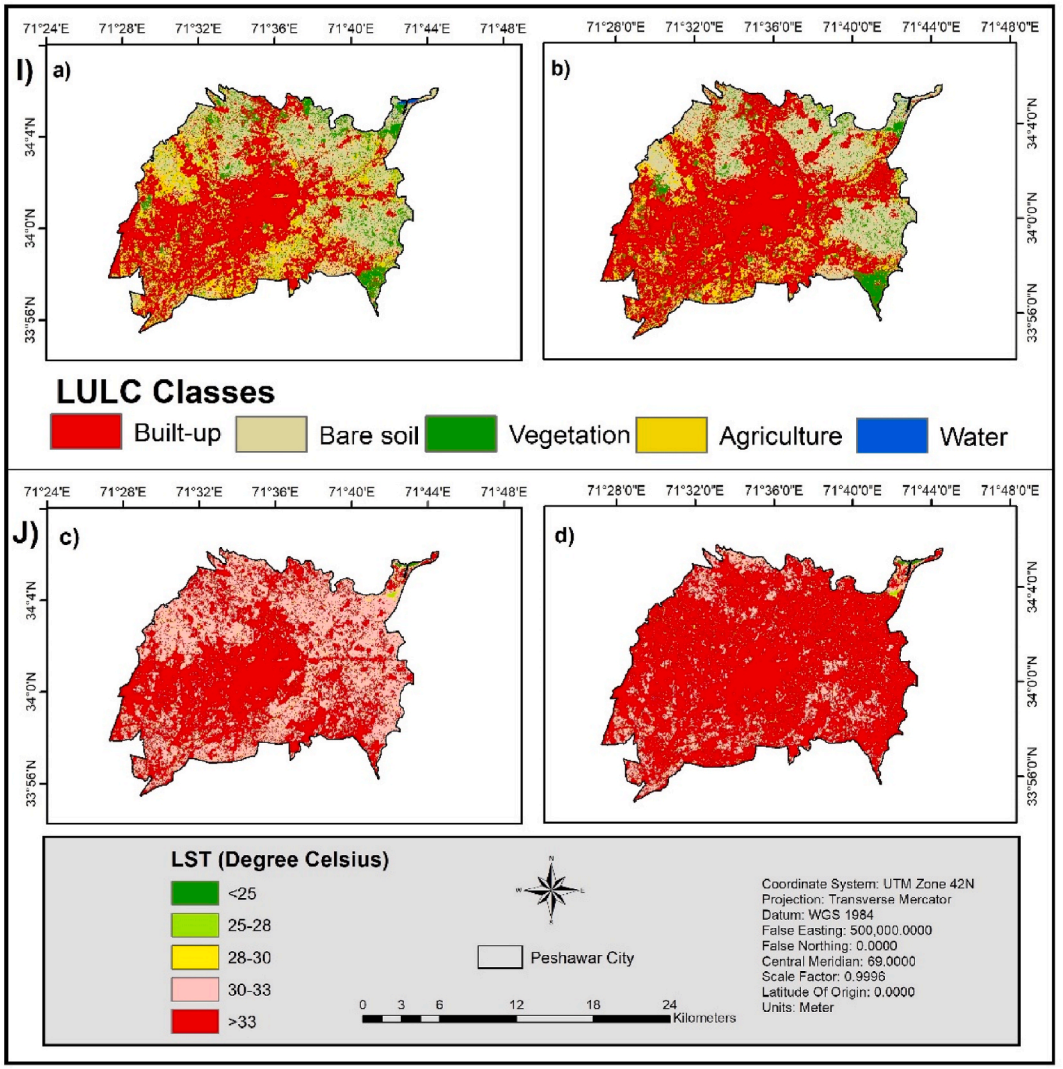

Fig. 7. Simulated LULC (I) and LST (J) maps of the study area for years (a,c) 2035 and (b,d) 2050.

expected (Table 8, Fig. 8).

Pakistan is climate climate-sensitive country and ranked among top ten in terms of the climate change vulnerability index [41]. The average annual temperature in Pakistan has increased by about 0.5 °C over the past 50 years and is expected a further increase in the future. The number of heat wave days/annum has increased by nearly five times compared with 30 years ago [41]. According to the Fifth IPCC Assessment Report [56] the rising average temperatures in South Asia may exceed the global average and disturb the glacier melting rates and precipitation trends. Even more alarming is the sixth assessment report of IPCC [42] which indicates the highest recorded LST. Urban sprawl along with other anthropogenic activities (like industrialization, economic activities, transportation, etc.) coupled with global warming will cause an abrupt increase in surface temperature in the study area. This will not only produce heat-related illnesses, the spread of vector-borne diseases, and fatalities [57,58] but will also accelerate the demand for cooling, which will lead to more energy consumption and greenhouse gas emissions [59]. Apart from this, the local hydrology, diversity, and other multiple ecosystems provided by the urban area will be negatively affected.

4.4. Model evaluation and limitations of the study

ANN and LR models have high accuracy in classification and predictions. These models can effectively be trained to capture the relationship between dependent and independent variables. The integration of CA with LR increases the suitability of LULC prediction by capturing the transitions and spatial inter-decencies with time. Due to their multi-layer structure, ANN has a strong learning capability in terms of prediction accuracy.

The limitations of the study include spatio-temporal resolution of Landsat data. Landsat satellite provides images after 16 days with

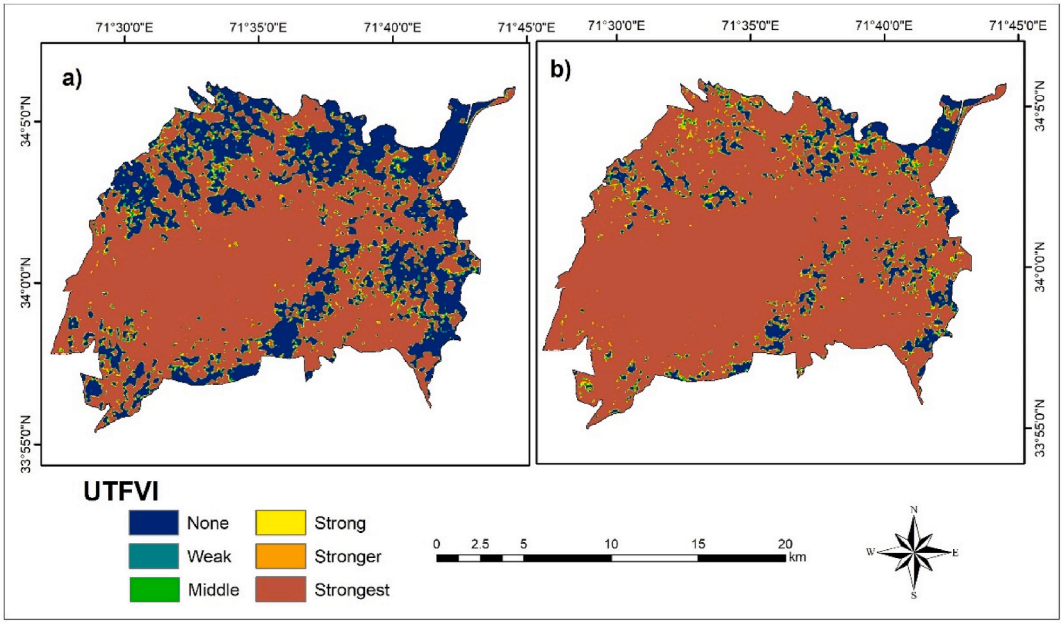

Fig. 8. Future simulated map showing UTFVI for the years a) 2035 and b) 2050 in the study area.

Table 8
Future simulated UTFVI for the years 2035 and 2050 in the study area.

UTFVI	Area (km^2)		Area (%)	
	2035	2050	2035	2050
None	86	20	27.48	6.39
Weak	10	8	3.19	2.56
Middle	5	5	1.60	1.60
Strong	8	6	2.56	1.92
Stronger	11	14	3.51	4.47
Strongest	193	260	61.66	83.07

a 30-m resolution. A more detailed analysis could be done with high-resolution images such as Sentinel (5-days & 10–15 m). Cloud cover sometimes obscures satellite images which compromises the accuracy of image classification and temperature analysis. The models i.e. LR and ANN are sensitive to overfitting if there are too many independent variables used or if the amount of training data is not sufficient. CA model can also be sensitive to spatial resolution of the input data which may lead to poor accuracy.

High-resolution satellite data may help to analyze the variation and trend in LULC and LST at the micro-scale with more detail. This study covers the gradient-direction analysis of urban, green spaces and LST. The same analysis can be done to study the effect of elevation, slope and aspect on LST in different directions and distance from the city center.

5. Conclusion

The main objective of the present study was to analyze the effect of changes in LULC on LST and UHI in Peshawar City from 1990 to 2020. The Artificial Neural Network (ANN) algorithm was applied to Landsat imageries to classify LULC into four classes i.e., built-up, bare soil, vegetation, and water bodies. Thermal bands of the selected Landsat imageries were used to calculate LST from 1990 to 2020. The results showed drastic changes in LULC from 1990 to 2020. Built-up areas showed a +22.07 % increase, while vegetation and bare soil decreased by −10.30 % and −11.68 % from 1990 to 2020. According to zonal analysis between LULC and LST, built-up areas showed the highest mean LST. This trend is followed by bare soil, vegetation, and water bodies. LULC and LST changes were simulated for 2035 and 2050 using CA-LR and ANN models. The future prediction results showed that built-up areas are expected to increase to 37.28 % and 49.60 % in 2035 and 2050, respectively. Similarly, the area associated with the LST class >33 °C is likely to increase to ~54 % and ~82 % in 2035 and 2050, respectively which was 48.47 % in 2020. The lower LST classes were noted to be shifted to higher which could be the reason for UHI formation in Peshawar City. The results of this study may be helpful for urban planners to control the unplanned urban growth in the study area. The effect of UHI may be controlled through urban planning. Planned urban areas can better control temperature as compared to unplanned urban areas. Furthermore, urban plantations and forests in the centers of the city are the best possible solution to mitigate the UHI formation. Land suitability analysis should be carried out to identify urban hotspots

and to design urban forestry.

Ethical Statement

On behalf of all authors, I assure that this manuscript needs no ethical consideration more than the necessary references.

Declaration

Dr. Adnan Ahmad Tahir (corresponding author) is related to Heliyon: Earth Section as an Associate Editor. Otherwise, the authors declare that there is no known competing financial interest or personal relationship that could have appeared to influence the work reported in this article.

Data availability

The data used in this research will be provided on request.

CRediT authorship contribution statement

Mudassir Khan: Writing – original draft, Validation, Software, Methodology, Formal analysis, Data curation, Conceptualization. **Muhammad Qasim:** Writing – review & editing, Investigation. **Adnan Ahmad:** Writing – review & editing, Investigation. **Adnan Ahmad Tahir:** Writing – review & editing, Validation, Supervision, Methodology, Formal analysis. **Abida Farooqi:** Writing – review & editing, Validation, Supervision, Methodology, Investigation, Formal analysis, Data curation, Conceptualization.

Declaration of competing interest

The authors declare the following financial interests/personal relationships which may be considered as potential competing interests:Associate Editor of the Heliyon: Earth Science section - Adnan Ahmad Tahir (corresponding author).If there are other authors, they declare that they have no known competing financial interests or personal relationships that could have appeared to influence the work reported in this paper.

References

[1] J.C. Hunt, et al., Climate change and growing megacities: hazards and vulnerability, in: Proceedings of the Institution of Civil Engineers-Engineering Sustainability, Thomas Telford Ltd, 2017.
[2] A. Guo, et al., Contribution of urban trees in reducing land surface temperature: evidence from China's major cities, Int. J. Appl. Earth Obs. Geoinf. 125 (2023) 103570.
[3] J. Ge, et al., Effects of urban vegetation on microclimate and building energy demand in winter: an evaluation using coupled simulations, Sustain. Cities Soc. 102 (2024) 105199.
[4] J.A. Salmond, et al., Health and climate related ecosystem services provided by street trees in the urban environment, Environ. Health 15 (2016) 95–111.
[5] M.T. Daramola, et al., Assessment of the thermal response of variations in land surface around an urban area, Model. Earth Syst. Environ. 4 (2018) 535–553.
[6] X. Gui, et al., Investigating the urbanization process and its impact on vegetation change and urban heat island in Wuhan, China, Environ. Sci. Pollut. Control Ser. 26 (2019) 30808–30825.
[7] K. Shang, et al., Study of urban heat island effect in Hangzhou metropolitan area based on SW-TES algorithm and image dichotomous model, Sage Open 13 (4) (2023) 21582440231208851.
[8] M. Mokarram, F. Taripanah, T.M. Pham, Investigating the effect of surface urban heat island on the trend of temperature changes, Adv. Space Res. 72 (8) (2023) 3150–3169.
[9] A. Liaqut, et al., Impact of urbanization growth on land surface temperature using remote sensing and GIS: a case study of Gujranwala City, Punjab, Pakistan, Int. J. Econ. Environ. Geol. 9 (3) (2018) 44–49.
[10] K.R. Gunawardena, M.J. Wells, T. Kershaw, Utilising green and bluespace to mitigate urban heat island intensity, Sci. Total Environ. 584-585 (2017) 1040–1055.
[11] A.M. Dewan, et al., Urbanisation and environmental degradation in Dhaka metropolitan area of Bangladesh, Int. J. Environ. Sustain Dev. 11 (2) (2012) 118–147.
[12] Mirzaei, P.A., Recent challenges in modeling of urban heat island, Sustain. Cities Soc. 19 (2015) 200–206.
[13] A.A. Kafy, et al., Modeling the relationship between land use/land cover and land surface temperature in Dhaka, Bangladesh using CA-ANN algorithm, Environ. Chall. 4 (2021) 100190.
[14] A. Ahmad, et al., Carbon emission from deforestation, forest degradation and wood harvest in the temperate region of Hindukush Himalaya, Pakistan between 1994 and 2016, Land Use Pol. 78 (2018) 781–790.
[15] S. Maithani, G. Nautiyal, A. Sharma, Investigating the effect of lockdown during COVID-19 on land surface temperature: study of Dehradun city, India, J. Indian Soc. Rem. Sens. 48 (2020) 1297–1311.
[16] D. Zhou, et al., Satellite remote sensing of surface urban heat islands: progress, challenges, and perspectives, Rem. Sens. 11 (1) (2018) 48.
[17] Q. Weng, A remote sensing? GIS evaluation of urban expansion and its impact on surface temperature in the Zhujiang Delta, China, Int. J. Rem. Sens. 22 (10) (2001) 1999–2014.
[18] P. Shahmohamadi, et al., The impact of anthropogenic heat on formation of urban heat island and energy consumption balance, Urban Stud. Res. 2011 (2011) 497524.
[19] P. Singh, et al., Impact of land use change and urbanization on urban heat island in Lucknow city, Central India. A remote sensing based estimate, Sustain. Cities Soc. 32 (2017) 100–114.
[20] C.I. Portela, et al., Impact of urban and industrial features on land surface temperature: Evidences from satellite thermal indices, Sustain. Cities Soc. 56 (2020) 102100.
[21] Z. Yin, et al., Urban heat islands and their effects on thermal comfort in the US: New York and New Jersey, Ecol. Indicat. 154 (2023) 110765.
[22] M.B. Moisa, D.O. Gemeda, Assessment of urban thermal field variance index and thermal comfort level of Addis Ababa metropolitan city, Ethiopia, Heliyon 8 (8) (2022) e10185.

[23] A.A. Kafy, et al., Assessing and predicting land use/land cover, land surface temperature and urban thermal field variance index using Landsat imagery for Dhaka Metropolitan area, Environ. Chall. 4 (2021) 100192.
[24] M. Nasar-u-Minallah, et al., Ecological monitoring of urban thermal field variance index and determining the surface urban heat island effects in Lahore, Pakistan, Environ. Monit. Assess. 195 (10) (2023) 1212.
[25] A.A. Kafy, et al., Predicting changes in land use/land cover and seasonal land surface temperature using multi-temporal landsat images in the northwest region of Bangladesh, Heliyon 7 (7) (2021) e07623.
[26] N.N. Dey, et al., Geospatial modelling of changes in land use/land cover dynamics using Multi-layer Perceptron Markov chain model in Rajshahi City, Bangladesh, Environ. Chall. 4 (2021) 100148.
[27] N. Kikon, D. Kumar, S.A. Ahmed, Analysing transition of land surface temperature and derived indices with respect to elevation values in Kohima Saddar, Geojournal 87 (Suppl 4) (2022) 821–846.
[28] M. Mokarram, F. Taripanah, T.M. Pham, Assessing air pollution changes during the COVID-19 and its impact on the urban environment using remote sensing and neural networks, Adv. Space Res. 73 (3) (2024) 1760–1779.
[29] M.S.H. Swapan, et al., Transforming urban dichotomies and challenges of South Asian megacities: rethinking sustainable growth of Dhaka, Bangladesh, Urban Sci. 1 (4) (2017) 31.
[30] A. Mannan, et al., Urban growth patterns and forest carbon dynamics in the metropolitan twin cities of Islamabad and Rawalpindi, Pakistan, Sustainability 13 (22) (2021) 12842.
[31] S. Salma, S. Rehman, M.A. Shah, Rainfall trends in different climate zones of Pakistan, Pak. J. Meteorol. 9 (17) (2012) 37–47.
[32] T. Kavzoglu, P.M. Mather, The use of backpropagating artificial neural networks in land cover classification, Int. J. Rem. Sens. 24 (23) (2003) 4907–4938.
[33] S. Lek, J.F. Guégan, Artificial neural networks as a tool in ecological modelling, an introduction, Ecol. Model. 120 (2–3) (1999) 65–73.
[34] J.F. Mas, Mapping land use/cover in a tropical coastal area using satellite sensor data, GIS and artificial neural networks, Estuar. Coast Shelf Sci. 59 (2) (2004) 219–230.
[35] D.A. Artis, W.H. Carnahan, Survey of emissivity variability in thermography of urban areas, Rem. Sens. Environ. 12 (4) (1982) 313–329.
[36] J.A. Sobrino, J.C. Jiménez-Muñoz, L. Paolini, Land surface temperature retrieval from LANDSAT TM 5, Rem. Sens. Environ. 90 (4) (2004) 434–440.
[37] M.S. Salama, et al., Decadal variations of land surface temperature anomalies observed over the Tibetan Plateau by the Special Sensor Microwave Imager (SSM/I) from 1987 to 2008, Clim. Change 114 (2012) 769–781.
[38] Z. Gao, et al., Toward park design optimization to mitigate the urban heat Island: Assessment of the cooling effect in five U.S. cities, Sustain. Cities Soc. 81 (2022) 103870.
[39] C. Agarwal, *A Review and Assessment of Land-Use Change Models: Dynamics of Space, Time, and Human Choice.* books.google.Com, 2002.
[40] V.N. Vapnik, An overview of statistical learning theory, IEEE Trans. Neural Netw. 10 (5) (1999) 988–999.
[41] R.A. Houghton, The worldwide extent of land-use change, BioScience 44 (5) (1994) 305–313.
[42] B. Yu, X. Zhou, Land finance and urban Sprawl: evidence from prefecture-level cities in China, Habitat Int. 148 (2024) 103074.
[43] L. Jiang, et al., Measuring the impact of government intervention on the spatial variation of market-oriented urban redevelopment activities in Shenzhen, China, Cities 147 (2024) 104834.
[44] C. Jiang, et al., Do adaptive policy adjustments deliver ecosystem-agriculture-economy co-benefits in land degradation neutrality efforts? Evidence from southeast coast of China, Environ. Monit. Assess. 195 (10) (2023) 1215.
[45] R.G. Pontius, M. Millones, Death to Kappa: birth of quantity disagreement and allocation disagreement for accuracy assessment, Int. J. Rem. Sens. 32 (15) (2011) 4407–4429.
[46] F. Haq, et al., Effectiveness of billion trees Tsunami afforestation projects in restoration of forests in Pakistan, Environ. Dev. Sustain. (2024).
[47] Z. Hassan, et al., Dynamics of land use and land cover change (LULCC) using geospatial techniques: a case study of Islamabad Pakistan, SpringerPlus 5 (2016) 812.
[48] D. Kumar, S. Shekhar, Statistical analysis of land surface temperature–vegetation indexes relationship through thermal remote sensing, Ecotoxicol. Environ. Saf. 121 (2015) 39–44.
[49] D. Kumar, Surface temperature variability analysis of an urban area using Landsat ETM+ thermal images, Asian Geogr. 34 (1) (2017) 25–37.
[50] C. Wang, et al., Urban vegetation cooling capacity was enhanced under rapid urbanization in China, J. Clean. Prod. 425 (2023) 138906.
[51] C. Wang, et al., Efficient cooling of cities at global scale using urban green space to mitigate urban heat island effects in different climatic regions, Urban For. Urban Green. 74 (2022) 127635.
[52] M. Shaygan, M. Mokarram, Investigating patterns of air pollution in metropolises using remote sensing and neural networks during the COVID-19 pandemic, Adv. Space Res. 72 (8) (2023) 3065–3081.
[53] S.M. Nizami, The inventory of the carbon stocks in sub tropical forests of Pakistan for reporting under Kyoto Protocol, J. For. Res. 23 (3) (2012) 377–384.
[54] A. Ahmad, S.M. Nizami, Carbon stocks of different land uses in the Kumrat valley, Hindu Kush Region of Pakistan, J. For. Res. 26 (2015) 57–64.
[55] I. Santé, et al., Cellular automata models for the simulation of real-world urban processes: a review and analysis, Landsc. Urban Plann. 96 (2) (2010) 108–122.
[56] R.K. Pachauri, et al., Climate Change 2014: Synthesis Report. Contribution of Working Groups I, II and III to the Fifth Assessment Report of the Intergovernmental Panel on Climate Change, IPCC, 2014.
[57] O. Brousse, et al., Using local climate zones in Sub-Saharan Africa to tackle urban health issues, Urban Clim. 27 (2019) 227–242.
[58] H.M. Moda, et al., Impacts of climate change on outdoor workers and their safety: some research priorities, Int. J. Environ. Res. Public Health 16 (18) (2019) 3458.
[59] N. Santillán-Soto, et al., Comparative analysis of two urban microclimates: energy consumption and greenhouse gas emissions, Sustainability 11 (7) (2019) 2045.